Non-Born-Oppenheimer dynamics of the photoionized Zundel cation: A quantum wavepacket and surface-hopping study

Zheng Li, Mohamed El-Amine Madjet, and Oriol Vendrell

Citation: The Journal of Chemical Physics **138**, 094313 (2013); doi: 10.1063/1.4793274
View online: http://dx.doi.org/10.1063/1.4793274
View Table of Contents: http://scitation.aip.org/content/aip/journal/jcp/138/9?ver=pdfcov
Published by the AIP Publishing

Non-Born-Oppenheimer dynamics of the photoionized Zundel cation: A quantum wavepacket and surface-hopping study

Zheng Li (李铮),[1,2,a)] Mohamed El-Amine Madjet,[1] and Oriol Vendrell[1,b)]
[1]*Center for Free-Electron Laser Science, DESY, Notkestrasse 85, D-22607 Hamburg, Germany*
[2]*Department of Physics, University of Hamburg, D-20355 Hamburg, Germany*

(Received 3 January 2013; accepted 8 February 2013; published online 5 March 2013)

The ultrafast fragmentation of the Zundel cation $H^+(H_2O)_2$ after photoionization is studied by quantum-dynamics with the multiconfiguration time-dependent Hartree method and with surface-hopping approaches. A picture emerges in which the correlated motion of the electron hole and the shared proton leads to localization of the two positively charged entities at opposite sides of the Zundel dication in less than 10 fs followed by Coulomb explosion. Electronic non-adiabatic effects play a crucial role in the fragmentation dynamics. The photoionization spectrum of the cluster between 20 and 24 eV is calculated quantum-dynamically and its features explained. Two- and three-body fragmentation channels accessible by outer-valence ionization are also calculated and the branching ratios as a function of ionization energy are discussed. A good agreement between the quantum-dynamical treatment and surface-hopping is obtained for observables for which both methods are applied. © *2013 American Institute of Physics*. [http://dx.doi.org/10.1063/1.4793274]

I. INTRODUCTION

The profound effect of non-adiabatic interactions between electronic states on the time-evolution of molecular systems has been one of the central focuses of excited state chemical dynamics.[1–5] The non-radiative decay of excited electronic states when a molecule approaches conical intersections or avoided crossings can result in a significant amount of energy redistribution into the vibrational modes or even in isomerization or fragmentation processes. Electronically excited molecules and clusters can be produced in various ways. One possibility is by strong-field ionization, in which several photons have to be absorbed before an electron leaves the system. This results in systems that are close to the ground electronic state of the ion. Another possibility is by one-photon absorption of extreme ultraviolet (XUV) or X-ray photons. This leaves the system potentially in a highly excited electronic state, which can even autoionize if the electronic energy is above the next ionization threshold of the system at hand. There is a large body of knowledge related to the dynamics and spectroscopic characterization of excited molecular systems after photoabsorption and photoionization.[6,7] However, not much is known about the nuclear dynamics and the role of non-adiabatic effects unfolding after XUV one-photon ionization of weakly bound clusters, for example, of water molecules.[8–10] In the case of weakly bound clusters, the charge produced by the ionization process may lead to a fast fragmentation of the system and to fast charge redistributions related to both electronic and nuclear degrees of freedom. Since clusters under such conditions may often fragment, non-Born-Oppenheimer (non-BO) effects lead to irreversible electronic relaxation processes in which the electronic excitation energy ends up as kinetic energy of the fragments.

For a theoretical treatment of such non-adiabatic dynamics, two essential ingredients are required. First, a set of reliable potential energy surfaces (PES) of the valence excited electronic states of the ionic system and their couplings and, second, an efficient approach to calculate the motion of atomic nuclei on that PES. Quantum mechanical wavepacket methods have established a rigorous basis for fully understanding the mechanisms of molecular processes.[11,12] However, in order to treat medium- or large-sized molecular systems fully quantum mechanically, one has to often make compromises to reduce the dimensionality due to limitations in computational power or to introduce model Hamiltonians. Even though it is possible to break the exponential scaling of wavepacket methods with, e.g., the multilayer multi-configurational time-dependent Hartree (ML-MCTDH) approach, these methods are still difficult to apply to non-model Hamiltonians.[13] If one is ready to compromise in the description of nuclear quantum effects, trajectory based approaches working in a Cartesian space, either based on Gaussian wavepackets,[12] and semiclassical[14] or mixed quantum-classical[15] approaches provide efficient computational strategies to treat medium to large molecular systems in full dimensionality. However, one must realize that their reliability may break down for processes out of their scope of applicability.[16]

In the present study, the Coulomb explosion of the protonated water dimer $H^+(H_2O)_2$ after ionization by XUV radiation has been investigated using quantum wavepackets and a mixed quantum-classical surface-hopping approach. Experiments on this fragmentation process had been performed at the free-electron laser (FEL) FLASH.[17] There, the fragmentation channels and their kinetic energies had been measured and a dominant two body fragmentation into $H_3O^+ + H_2O^+$

a)zheng.li@cfel.de.
b)oriol.vendrell@cfel.de.

was found. Previous wavepacket studies have demonstrated important non-adiabatic effects during the fragmentation of the cluster due to the presence of multiple conical intersections in the Franck-Condon region upon ejection of a valence electron.[18] There, we could show that, upon ionization, an ultrafast localization of a shared proton and the electron hole at opposite sides of the cluster takes place, in which non-adiabatic effects play a key role, immediately followed by Coulomb explosion. The wavepacket studies in Ref. 18 focused on the three lowest outer valence electronic excitations of the cluster. Here, we extend those calculations to the complete outer valence shell, which for the Zundel cation means six electronic states. This opens up new three- and four-body fragmentation channels that do not occur from lower excited states. Besides a fundamental understanding of the ultrafast fragmentation mechanism, we provide a detailed comparison of wavepacket and surface-hopping calculations as well on the same PES and compare them in the context of several observable quantities. The paper is organized as follows. Section II reviews the theoretical framework of both the wavepacket and mixed-quantum classical calculations, as well as the calculation of the PES. Section III A discusses the topology and crossings of the involved PES. Section III B presents the results of the dynamics calculations and discusses the ultrafast fragmentation process. Sections III C and III D discuss the photoionization (PI) and kinetic energy release (KER) spectra, and Sec. III E covers the dynamics from the upper outer-valence states. Finally, Sec. IV concludes and provides some outlook for future work.

II. THEORETICAL FRAMEWORK

A. Adiabatic potential energy surfaces of the $H_5O_2^{2+}$ dication

For the quantum-dynamical calculations of $H_5O_2^{2+}$, the system is described by a mixed set of polyspherical Jacobi-valence coordinates. The definition of the polyspherical coordinates is described in detail in previous work.[19] The chosen coordinate system is known to be advantageous for treating large amplitude motions.[20] The set of polyspherical vectors is shown in Fig. 1. From the full set of 15 nuclear coordinates that describe the geometry of the cluster, we choose a reduced set of 7 coordinates consisting of $\{x, y, z, R, \alpha, \gamma_A, \gamma_B\}$, where R is the distance between oxygen atoms of the two water monomers, the Cartesian coordinates (x, y, z) describe the position of the central proton with origin set at the center of mass of the two oxygen atoms, and α (internal relative rotation) and $\gamma_{(A,B)}$ (waggings) represent the Euler angles defining the relative orientation of the two water monomers. The internal degrees of freedom of the water monomers and their rocking motion, which possess higher moments of inertia than that of wagging motion, were chosen to be frozen at the equilibrium positions in the Franck-Condon region. We also adopt the definition of the dimensionless z coordinate[21]

$$z \mapsto \frac{z}{R - 2d_0}, \tag{1}$$

which in this case with large separations of the monomers is crucial in order to adequately avoid molecular configurations with the central proton unphysically close to the oxygen atoms. In Eq. (1), d_0 is chosen to be the covalent radius of the oxygen atom, 0.65 Å.

We proceed by calculating the adiabatic PES on the 7D grid of the coordinates mentioned above. As detailed in Sec. II B, we then diabatize *point-by-point* based only on the energy values on the grid. We apply this strategy instead of, e.g., using a vibronic-coupling Hamiltonian with a fixed expansion point because of the large amplitude motions taking place during the fragmentation. Due to the large number of points in the 7D grid we construct adiabatic *ab initio* PES for the ionized states of $H_5O_2^{2+}$ using a high level-low level approach

$$V_i(\mathbf{Q}) = V_{i,\text{high}}(\mathbf{a}; x, y, z, R) + (V_{i,\text{low}}(\mathbf{Q}) - V_{i,\text{low}}(\mathbf{a}; x, y, z, R)), \tag{2}$$

where i refers to the adiabatic electronic state. The high level electronic structure calculations are hence performed in the 4D subspace of the central proton displacements and the oxygen-oxygen distance coordinates. As will be discussed later, these degrees of freedom are the key ones to describe the fragmentation process and the involved conical intersections. In the high-level calculations the spectator degrees of freedom α, γ_a, and γ_b are set at reference positions where $\mathbf{a} = \{\alpha_0, \gamma_{a,0}, \gamma_{b,0}\}$ corresponding to the equilibrium geometry of $H^+(H_2O)_2$ within the D_{2d} point group. In order to accurately describe the excited state PES of $H_5O_2^{2+}$ in the high level subspace we use the complete active space self-consistent field (CASSCF) method[22,23] employing the cc-pVTZ basis set.[24] We use an active space with 11 electrons distributed in 8 molecular orbitals. For selected cuts we investigated the effect of including dynamical correlation at the CASPT2 level, but the change in shape of the PES was found to be small. The low-level calculations were performed at the Hartree-Fock-Koopmans (HF-K) level

$$V_{i,\text{HF-K}} = V_{\text{HF}} - \epsilon_i, \tag{3}$$

where V_{HF} is the ground state Hartree-Fock energy of $H^+(H_2O)_2$ and ϵ_i is the energy of the ith orbital counting from the highest occupied molecular orbital downwards. The two-level scheme is similar in spirit to an n-mode representation of the PES,[19,25,26] in which the largest possible cluster (7D) is present but computed at a lower level of theory than smaller clusters.

The surface-hopping trajectory calculations discussed below were performed on CASSCF PES and gradients

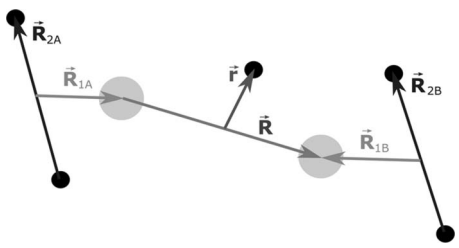

FIG. 1. Mixed Jacobi-valence description of the $H_5O_2^{2+}$ system. The two big circles represent the position of the oxygen atoms, while the small circles represent the positions of the hydrogen atoms.

obtained *on the fly* using the same active space as above. All CASSCF calculations were performed with the quantum chemistry package MOLCAS.[27]

B. Diabatization of the Hamiltonian

To describe the fragmentation dynamics of $H_5O_2^{2+}$ on the three lowest outer-valence electronic states by quantum dynamics, we construct the Hamiltonian in a diabatic representation from the adiabatic PES discussed above. In the diabatic representation we eliminate the diverging part of the derivative couplings of the kinetic energy term that would appear in the adiabatic Hamiltonian operator,[1] which is singular at the conical intersections. The total Hamiltonian in the diabatic representation can be written as

$$\mathbf{H} = T_{\mathrm{N}}\mathbf{1} + \mathbf{W}, \tag{4}$$

where T_{N} is the nuclear kinetic energy operator (KEO). The potential energy matrix $\mathbf{W}$ is constructed relying on a regularized diabatization scheme[28–31] discussed below.

We first adopt symmetry-adapted coordinates classified with respect to the D_{2d} point group, in order to take advantage of the fact that the coordinates responsible for the linear nonadiabatic coupling should satisfy the condition

$$\Gamma_s \otimes \Gamma_{s'} \otimes \Gamma_\alpha \supset A_g, \tag{5}$$

where Γ_s, $\Gamma_{s'}$, Γ_α are the irreducible representations of the electronic states and nuclear coordinates, respectively.[28] The working equation for the regularized diabatic potential energy matrix for a two-states problem reads[28]

$$\mathbf{W}^{\alpha\beta} = \Sigma^{\alpha\beta}\mathbf{1} + \frac{\Delta^{\alpha\beta}(\mathbf{Q}_g, \mathbf{Q}_u)}{\sqrt{\frac{\left(\Delta_0^{\alpha\beta}\right)^2}{4} + (\lambda^{\alpha\beta}\cdot\mathbf{Q}_u)^2}} \times \begin{pmatrix} -\frac{\Delta_0^{\alpha\beta}}{2} & \lambda^{\alpha\beta}\cdot\mathbf{Q}_u \\ \lambda^{\alpha\beta}\cdot\mathbf{Q}_u & -\frac{\Delta_0^{\alpha\beta}}{2} \end{pmatrix}, \tag{6}$$

where $\mathbf{Q}_g$ and $\mathbf{Q}_u$ represent the sets of totally symmetric and nontotally symmetric vibrational modes, respectively, α, β are electronic state indices, $\Sigma^{\alpha\beta}$ is the mean energy of both adiabatic PES, $\Delta_0^{\alpha\beta} = \Delta V_0^{\alpha\beta}$ is the energy difference between adiabatic PES V^α and V^β in the reference coordinate subspace, and the coupling constants $\lambda_i^{\alpha\beta}$ were determined according to[5]

$$\lambda_i^{\alpha\beta} = \left\{ \frac{1}{8}\frac{\partial^2}{\partial Q_u^2}(V^\beta(Q_g, Q_u) - V^\alpha(Q_g, Q_u))^2 \right\}^{\frac{1}{2}}\Bigg|_{Q_g;Q_u=0}. \tag{7}$$

To construct the linear coupling matrix in Eq. (6), the coordinates were grouped by their associated representations. $G_1 \equiv (\frac{1}{\sqrt{2}}(x \pm y), R, \frac{1}{\sqrt{2}}(\gamma_A \pm \gamma_B))$ and $G_3 \equiv (R, z, \alpha)$ are the sets of modes that directly enter the diagonal potential matrix elements, $G_2 \equiv (z, \alpha)$ and $G_4 \equiv (\frac{1}{\sqrt{2}}(x \pm y), \frac{1}{\sqrt{2}}(\gamma_A \pm \gamma_B))$ are the modes responsible for the off-diagonal linear couplings between different electronic states. The coordinates in groups G_1 and G_2 are for pair of states (1,2), the coordinates in groups G_3 and G_4 are for pairs of states (1,3) and (2,3).

We then apply the regularized-states procedure of Eq. (6) to the three adiabatic states in pairs first. The submatrix that couples diabatic states 1 and 2 is kept. From the submatrices for states (1, 3) and (2, 3), we keep only the corresponding W_{13} and W_{23}, and the two W_{33} elements are averaged. Now the elements W_{13} and W_{23} from the latest diagonalization correspond to states 1 and 2 that have not been mixed among each other. We resolve this by applying the transformation

$$\begin{pmatrix} \tilde{W}_{13} \\ \tilde{W}_{23} \end{pmatrix} = U \begin{pmatrix} W_{13} \\ W_{23} \end{pmatrix}, \tag{8}$$

such that the new coupling elements now connect the diabatic state 3 to the diabatic states 1 and 2 obtained from the first diabatization procedure. In Eq. (8), the 2×2 matrix $\mathbf{U}$ is the transformation matrix that diagonalizes the sub-potential-matrix $\mathbf{W}^{(12)}$ for the lowest two diabatic states, i.e., $\mathbf{U}^\dagger\mathbf{W}^{(12)}\mathbf{U} = V^{(12)}$.

The potential energy matrix $\mathbf{W}$ in diabatic representation is finally regularized through

$$\mathbf{W}^{\mathrm{reg}} = \mathbf{S}\mathbf{V}^{(ab\ initio)}\mathbf{S}^\dagger, \tag{9}$$

where $\mathbf{S}$ is the transformation matrix that diagonalizes $\mathbf{W}$, i.e., $\mathbf{S}^\dagger\mathbf{W}\mathbf{S} = \mathbf{V}$. The main purpose of this last regularization procedure is to ensure that the *ab initio* potential energy data $\mathbf{V}^{(ab\ initio)}$ in the adiabatic representation is fully reproduced via the inverse transformation from the diabatic representation used in the calculations.[28] This transformation does not change the diabatic matrix to first order near the conical intersections.

After construction of the regularized diabatic potential energy matrix $\mathbf{W}_{\mathrm{reg}}$, the final Hamiltonian in the diabatic representation is obtained by adding the nuclear KEO into Eq. (4). For the sake of simplicity, we do not distinguish $\mathbf{W}$ from $\mathbf{W}^{\mathrm{reg}}$ in the following.

C. The multi-configurational time-dependent Hartree method

The MCTDH method[11,32,33] is a highly efficient approach to solve the time-dependent Schrödinger equation. The MCTDH-*ansatz* for the nuclear wavefunction is briefly discussed in the following for completeness.

The MCTDH wave function is expanded in Hartree products of time-dependent basis functions called *single-particle functions* (SPFs). The SPFs, $\varphi(Q, t)$, may be one- or multi-dimensional functions. In the latter case, the coordinate Q is a collective mode comprising several degrees of freedom $Q = (q_k, \ldots, q_l)$. The MCTDH *ansatz* for wavefunction reads

$$\begin{aligned} \Psi(q_1, \ldots, q_f, t) &\equiv \Psi(Q_1, \ldots, Q_p, t) \\ &= \sum_{j_1}^{n_1} \cdots \sum_{j_p}^{n_p} A_{j_1,\cdots,j_p}(t) \prod_{\kappa=1}^{p} \varphi_{j_\kappa}^{(\kappa)}(Q_\kappa, t) \\ &= \sum_J A_J \Phi_J, \end{aligned} \tag{10}$$

where f denotes the number of degrees of freedom and p the number of MCTDH combined modes. There are n_κ SPFs for the κth combined mode. The $A_J \equiv A_{j_1,\cdots,j_p}$ denote the MCTDH expansion coefficients and the configurations Φ_J are products of the time-dependent SPFs. The SPFs are finally represented by linear combinations of time-independent primitive basis functions or discrete variable representation (DVR) grids. The MCTDH equations of motion read

$$i\dot{A}_J = \sum_L \langle \Phi_J | H | \Phi_L \rangle A_L, \tag{11}$$

$$i\dot{\varphi}^{(\kappa)} = (1 - P^{(\kappa)})(\rho^{(\kappa)})^{-1}\langle \mathbf{H} \rangle^{(\kappa)} \varphi^{(\kappa)}, \tag{12}$$

where a vector notation, $\varphi^{(\kappa)} = (\varphi_1^{(\kappa)}, \cdots, \varphi_{n_\kappa}^{(\kappa)})^T$, is used. Details on the derivation, the definitions of the mean field $\langle \mathbf{H} \rangle^{(\kappa)}$, the density matrix $\rho^{(\kappa)}$, and the projector $P^{(\kappa)}$ can be found in Ref. 11.

The computational gain of the MCTDH method is acquired via keeping the number of SPF basis optimally small, i.e., the so-called MCTDH contraction effect. Because the SPFs are variationally optimized via the MCTDH equations of motion derived by applying the Dirac-Frenkel variational principle, they are ensured to evolve temporally in an optimal manner to describe the wave packet, therefore often a rather small number of SPFs suffices to achieve convergence. The efficiency can be further enhanced by combining several correlated degrees of freedom into one physical mode Q_i.

The solution of the MCTDH equations of motion demands efficient evaluation of the mean fields at every time step. To this end the Hamiltonian is represented as a sum of products of single mode operators, via the POTFIT method,[11,34,35] which allows us to bring a general PES into product form comprised of basis functions called *single-particle potentials* (SPPs).

The multi-electronic state wave functions can be written as

$$\Psi(Q_1, \ldots, Q_p, t) = \sum_{\alpha=1}^{n_s} \Psi_\alpha(Q_1, \ldots, Q_p, t) |\alpha\rangle, \tag{13}$$

where n_s is the number of electronic states. We have applied the multi-state formulation of MCTDH, in which a separate set of SPFs is propagated for every electronic state,[36] which are then coupled by the off-diagonal elements of the diabatic Hamiltonian.

The ground state vibrational wavefunction of the $H^+(H_2O)_2$ cation was obtained on the ground state PES employing the *improved relaxation* method.[37] This method converges faster than a simple imaginary time propagation and is essentially a multi-configuration self-consistent field approach that takes advantage of the MCTDH machinery.[19,38]

The acquired ground state wave function was then directly transferred to the excited states of the ionized $H_5O_2^{2+}$ dication as the initial wavepacket, assuming sudden ionization of the $H^+(H_2O)_2$ cation by the FEL pulse and validity of the Franck-Condon principle,[39] as schematically depicted in Fig. 3. The wavepacket dynamics on the excited state potentials were propagated up to 100 fs. Within a time period of ~65 fs the major photofragmentation process of the Zundel cation was observed in the present calculation, yet we carried out 100 fs quantum dynamical propagation to enable full absorption of the wave packet by the complex absorbing potentials (CAPs) for the purpose of flux analysis.

TABLE I. Definition of the one-dimensional grids. N denotes the number of grid points and x_i, x_f are the location of the first and the last point. The DVRs are defined in Appendix B of Ref. 11 (radial degrees of freedom are given in atomic units, while angular degrees of freedom are given in radians).

Coordinates	N	x_i	x_f	DVR
x	21	−3.0	3.0	sin
y	21	−3.0	3.0	sin
R	360	3.9	15.5	sin
z	63	−0.5	0.5	sin
α	26	0	2π	exp
γ_A	21	−1.8	1.8	sin
γ_B	21	π −1.8	π+1.8	sin

In order to enhance the efficiency of the MCTDH calculation, we made use of mode-combination using the following four combined modes $Q_1 = [x, y]$, $Q_2 = [z, \alpha]$, $Q_3 = [R]$, and $Q_4 = [\gamma_A, \gamma_B]$. The definition of the underlying one-dimensional (1D) grids and the DVR is provided in Table I. Table II contains the numbers of SPFs used for each degree of freedom in the MCTDH relaxation and dynamics calculations, which gives converged dynamical results.

In the present calculation, the CAPs were applied to x, y, R, γ_A, and γ_B coordinates in order to absorb the outgoing wavepacket. The CAP V_c for coordinate q_i takes the form[40]

$$V_c(q_i) = -i\eta |q_i - q_{i,c}|^n \theta(|q_i - q_{i,c}|), \tag{14}$$

where the strength parameter η, the order n, and the threshold $q_{i,c}$ were chosen so as to minimize the reflection from the CAP along the coordinate q_i. The suitably chosen CAP parameters were listed in Table II.

From the time-dependent wavepacket propagations, various properties were extracted. Since the wavepacket propagations were performed in a diabatic representation, the diabatic electronic state populations $P_\alpha(t)$ and the reduced densities $\rho_\alpha(q_i, q_j, t)$ of the wavepacket for the electronic state $|\alpha\rangle$ can be readily obtained as

$$P_\alpha(t) = \langle \Psi_\alpha(t) \mid \Psi_\alpha(t) \rangle \tag{15}$$

and

$$\rho_\alpha(q_i, q_j, t) = \int \Psi_\alpha^*(t)\Psi_\alpha(t) \prod_{l \neq i,j} dq_l, \tag{16}$$

TABLE II. Details of the MCTDH calculation. For each combined mode Q_i, the number of single particle functions (SPFs) and the parameters for the complex absorbing potentials (CAPs) of the form $V_c(q_i) = -i\eta|q_i - q_{i,c}|^n\theta(|q_i - q_{i,c}|)$ are given. The CAP parameters were listed as $(q_{i,c}, \eta, n)_{q_i}$. Atomic units are used for radial degrees of freedom, while radians are used for angular degrees of freedom.

Combined modes	Numbers of SPFs	CAP parameters
$Q_1 = [x, y]$	10	$(\pm 2.50, 0.05, 3)_{x,y}$
$Q_2 = [z, \alpha]$	10	z, α are CAP free
$Q_3 = [R]$	5	$(12.30, 0.005, 3)_R$
$Q_4 = [\gamma_A, \gamma_B]$	5	$(\pm 1.65, 0.05, 3)_{\gamma_A}$, $(\pi \pm 1.65, 0.05, 3)_{\gamma_B}$

respectively. In order to facilitate the comparison with surface-hopping calculations, where the electronic populations are expressed in terms of adiabatic electronic states, we also calculate the *adiabatic populations*.[41] For this, the wavepacket in adiabatic representation $\Psi_{\text{adiabatic}}$ is obtained by unitary transformation from the diabatic representation by

$$\Psi_{\text{adiabatic}} = \mathbf{S}^{\dagger}\Psi_{\text{diabatic}}, \tag{17}$$

where $\mathbf{S}$ is the position dependent transformation matrix of adiabatic-diabatic representations defined in Eq. (9).

D. The non-adiabatic surface-hopping method

The molecular wavefunction at a given time t can be expanded in the adiabatic representation as[1]

$$\Psi(\mathbf{r}_e; \mathbf{R}_N, t) = \sum_J \chi_J^N(\mathbf{R}_N, t)\phi_J^e(\mathbf{r}_e; \mathbf{R}_N), \tag{18}$$

where $\mathbf{r}_e$ is the collective coordinate of all electrons, and $\mathbf{R}_N$ is the one of the nuclei. $\chi_J^N(\mathbf{R}_N, t)$ and $\phi_J^e(\mathbf{r}_e; \mathbf{R}_N)$ correspond to the nuclear and electronic wavefunctions of the Jth electronic state, respectively.

In the context of surface hopping, the nuclear wavefunction $\chi_J^N(\mathbf{R}_N, t)$ is replaced by a swarm of M points in phase space with initial distribution that is analogous to the quasi density distribution of the corresponding wavefunction, namely each of the nuclear trajectories evolves independently and the quantum correlation between them is neglected. In this case, the nuclear wavefunction is considered to have the following quantum probability:[42]

$$\left|\chi_J^N(\mathbf{R}_N, t)\right|^2 = \frac{1}{M}\sum_\alpha \int_0^\infty dt' \left|C_J^{N,\alpha}(t')\right|^2 \delta(\mathbf{R}_N - \mathbf{R}_N^\alpha(t'))\delta(t - t'), \tag{19}$$

where $|C_J^{N,\alpha}(t')|^2$ is the probability to observe the nuclei with position $\mathbf{R}_N^\alpha$ at time t' in the αth trajectory. Under the assumption of independent trajectories, the molecular wavefunction is reduced to

$$\Psi^\alpha(\mathbf{r}_e, \mathbf{R}_N) = \sum_J C_J^{N,\alpha}(t)\phi_J^e(\mathbf{r}_e; \mathbf{R}_N) \tag{20}$$

for the αth trajectory.

In order to correctly depict the non-adiabatic relaxation dynamics of electrons associated to the nuclear motion, through which energy of electrons is either extracted from or pumped into the kinetic energy of nuclei, the surface hopping approaches utilize a procedure to switch the electronic PES on which the molecular nuclei move.

In the context of the Landau-Zener scheme,[43–45] the electronic population dynamics is fully determined by local topologies of the potential energy surfaces. The quantum-classical Landau-Zener formula for transition probability between adiabatic electronic states I and J is

$$P_{I,J}^{LZ} = \exp\left(-2\pi \frac{\Delta E_{IJ}^{a\,2}}{\hbar|\dot{\mathbf{R}}_N \cdot \vec{\nabla}\Delta E_{IJ}^d|}\right), \tag{21}$$

where $\vec{\nabla}\Delta E_{IJ}^d$ is the gradient of the energy difference between two diabatic electronic states I and J and ΔE_{IJ}^a is the energy difference between two adiabatic electronic states I and J. It is natural to expect that the transition probability should be maximized for small energy gap and large slope of the PESs as they come close. The implementation we used here for the Landau-Zener approach closely follows that of Jones *et al.*[43]

On the other side, the fewest-switches scheme[15,46] puts stress on the electronic coherence by explicitly incorporating the temporal evolution of electronic Schrödinger equation, which reads

$$i\hbar\dot{C}_J^{N,\alpha}(t) = \sum_I C_I^{N,\alpha}(t)\left(H_{JI} - i\hbar\dot{\mathbf{R}}_N^\alpha \cdot \mathbf{d}_{JI}^\alpha\right), \tag{22}$$

where $\mathbf{d}_{JI}^\alpha$ is the non-adiabatic coupling vector $\langle\phi_J^e(\mathbf{r}_e, \mathbf{R}_N)|\vec{\nabla}_{\mathbf{R}}|\phi_I^e(\mathbf{r}_e, \mathbf{R}_N)\rangle$. The matrix element $H_{JI} = \delta_{JI}E_J^e$ is diagonal in the adiabatic representation, where E_J^e is the electronic potential energy of the Jth state in the adiabatic representation. The non-adiabatic coupling matrix elements $\sigma_{JI} = \dot{\mathbf{R}}_N^\alpha \cdot \mathbf{d}_{JI}^\alpha = \langle\phi_J^e|\frac{\partial\phi_I^e}{\partial t}\rangle$ are calculated numerically by finite difference from the overlap of wave functions[47–49]

$$\sigma_{JI}(t + \Delta t/2) = \frac{1}{2\Delta t}\left[\left\langle\phi_J^e(t)\middle|\phi_I^e(t + \Delta t)\right\rangle - \left\langle\phi_J^e(t + \Delta t)\middle|\phi_I^e(t)\right\rangle\right], \tag{23}$$

with linear interpolation within a integration time step Δt.

The FSSH scheme generally keeps the number of switching events to be minimal (i.e., *fewest switches*), with the following probability g_{IJ} for the hopping from the Ith state to the Jth state within the time interval $[t, t + dt]$,[46]

$$g_{IJ}^\alpha(t, t + dt) = -2\int_t^{t+dt} d\tau \frac{\Re\left[C_J^{N,\alpha}(\tau)C_I^{*N,\alpha}(\tau)\dot{\mathbf{R}}_N^\alpha \cdot \mathbf{d}_{JI}^\alpha\right]}{C_I^{*N,\alpha}(\tau)C_I^{N,\alpha}(\tau)}. \tag{24}$$

Suppose ζ is a uniform random number between 0 and 1. A hopping event is invoked when the following inequality

$$\sum_{K\le J-1} g_{IK}^\alpha < \zeta < \sum_{K\le J} g_{IK}^\alpha, \tag{25}$$

as well as the energy conservation condition, is satisfied. In our implementation of Landau-Zener and fewest-switches schemes, the momentum of the nuclei are corrected immediately after the hopping by

$$\mathbf{p} \to \mathbf{p} + \mathbf{n}\left(\frac{\mathbf{n}M^{-1}\mathbf{p}}{\mathbf{n}M^{-1}\mathbf{n}}\right)\left(1 - \sqrt{1 - 2\Delta E\frac{\mathbf{n}M^{-1}\mathbf{n}}{(\mathbf{n}M^{-1}\mathbf{p})^2}}\right) \tag{26}$$

in order to conserve total energy and angular momentum, where M is the mass matrix, $\mathbf{n} = \mathbf{g}/|\mathbf{g}|$, and $\mathbf{g}$ is the gradient of the energy gap $\mathbf{g} = \vec{\nabla}_{\mathbf{R}}(E_J - E_I)$.[50]

Both the Landau-Zener and the fewest-switches schemes guarantee that the nuclei feel the force on a single electronic PES when the system leaves the interaction regions of strong non-adiabatic coupling. This scenario is physically consistent with the fact that in experiment the outgoing molecular fragments should be generally observed to sit on a single electronic state at the asymptotic region, rather than to maintain superposition of electronic states.

For the purpose of studying the influence of dimensionality to the surface-hopping quantum-classical dynamics, we applied the RATTLE scheme[51] to impose internal constraints on motions of atomic nuclei. In this way, we can precisely study the same reduced dimensionality model by both surface hopping and quantum dynamics.

Working with Cartesian coordinates, the rigid constraints are maintained by introducing implicit forces based on Lagrange multipliers. The equation of motion for atom i thus reads

$$m_i \ddot{\mathbf{R}}_{\mathrm{N},i} = \mathbf{F}_i + \mathbf{G}_i, \tag{27}$$

where $\mathbf{F}_i$ is the inherent force from electronic potential energy surface and $\mathbf{G}_i$ is the force on atom i in order to satisfy the constraints. $\mathbf{G}_i$ is given by

$$\mathbf{G}_i = -\sum_{\alpha} \lambda_{i\alpha} \vec{\nabla}_i \sigma_{i\alpha}(\{\mathbf{R}_{\mathrm{N}}(t)\}), \tag{28}$$

where $\sigma_{i\alpha}\{\mathbf{R}_{\mathrm{N}}(t)\} = 0$ are the set of general holonomic constraints imposed on atom i, which could be functions of either Cartesian or internal coordinates while their Cartesian derivatives $\vec{\nabla}_i \sigma_{i\alpha}(\{\mathbf{R}_{\mathrm{N}}(t)\})$ are evaluated by stable numerical differentiation, and $\lambda_{i\alpha}$ are time-dependent Lagrange multipliers associated with the force of constraints, which are determined by the iterative procedure of Andersen.[51] Since the constraint forces are by construction always orthogonal to the velocity vectors of atomic nuclei, they do not impose any work on the molecular system, and the total energy conservation is guaranteed.

The initial conditions for the Zundel cation were sampled from a Boltzman distribution in the phase space on the ground electronic PES. Care was taken to reproduce the quantum distribution along z by adjusting the sampling temperature. In future works we may consider sampling from a Wigner distribution of the ground vibrational state.

III. RESULTS AND DISCUSSION

A. Ground and lowest excited electronic states of $H_5O_2^{2+}$

For the dication $H_5O_2^{2+}$, one can depict the initial electron hole in the molecule by inspecting the molecular orbital from which a valence electron is ionized, i.e., applying the Koopmans theorem.[52] In the context of multi-configuration wavefunctions, for each of the low lying electronic states we could always identify one one-hole configuration with a population of more than 90% in the respective electronic state. This indicates that a one-particle picture description is adequate for the states under consideration. In particular in Fig. 2, we present the molecular orbitals corresponding to the electron hole in the lowest three electronic states of the dication. The two lowest-energy states can be depicted as removing an electron from a lone electron pair in either water molecule, while the third state corresponds to removing an electron from the hydrogen bond.

It is convenient to label the electronic states of interest using the C_{2v} point group as reference. The lowest two states are energetically degenerate when the molecule is close to

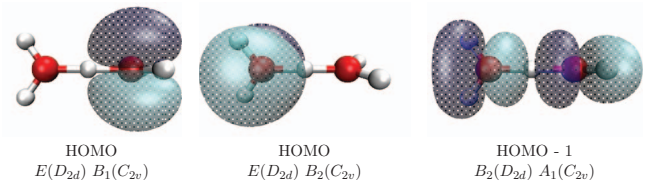

FIG. 2. The highest three occupied molecular orbitals of B_2, E, and E symmetries for the $H^+(H_2O)_2$ Zundel cation at D_{2d} symmetric configuration, from which the valence electron is photoionized. In the C_{2v} point group, these states correlate to the labels B_1, B_2, and A_1, respectively.

the absolute minimum in the electronic ground state of the Zundel cation, where they belong to the E irreducible representation within D_{2d} group, the degeneracy is lifted in first order along the proton-transfer coordinate of B_2 symmetry, resulting in a $E \otimes b$ conical intersection. Intuitively, when the central proton is displaced towards, e.g., the water molecule on the left, the electronic state with the hole on the water molecule of the right side gets stabilized, while the state with the hole on the left side is destabilized, leading to the lifting of the degeneracy. The third electronic state of the dication can be described by an electron hole extending mostly around the central hydrogen bond. Therefore, the PES is relatively flat along the proton-transfer coordinate in the vicinity of the Franck-Condon point. When the proton is displaced towards either water molecule, the electron hole eventually becomes more stable on the water molecule opposite to the proton side and at that geometry the third dicationic state crosses with the second one, resulting in new seams of conical intersections. This topology can be seen in Fig. 3. The Coulomb repulsion between the proton and the electron hole, which are both positively charged, further drives the molecular fragments carrying one of them to separate from each other. In this way, the electronic motion reacts on the nuclei, while the nuclear motion drives non-adiabatic electronic transitions. It

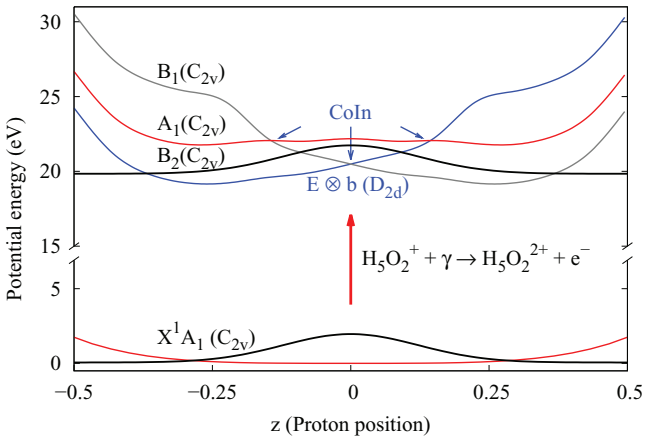

FIG. 3. A schematic view of the initial photoionization process of the $H^+(H_2O)_2$ cation. The potential energy curves, labeled by B_1, B_2, and A_1, respectively, for the excited electronic states of the ionized $H_5O_2^{2+}$ dication and the ground electronic state of the $H^+(H_2O)_2$ cation (X^1A_1) are depicted as a function of proton position z. The black curves correspond to the probability density of the ground vibrational state along the z coordinate. It can be seen that upon photoionization the system has non-negligible probability to be found directly on top of the region of conical intersection of the electronic states of the dication. The origin of the potential energy was set to the energy of $H^+(H_2O)_2$ cation at its equilibrium geometry on the ground state PES.

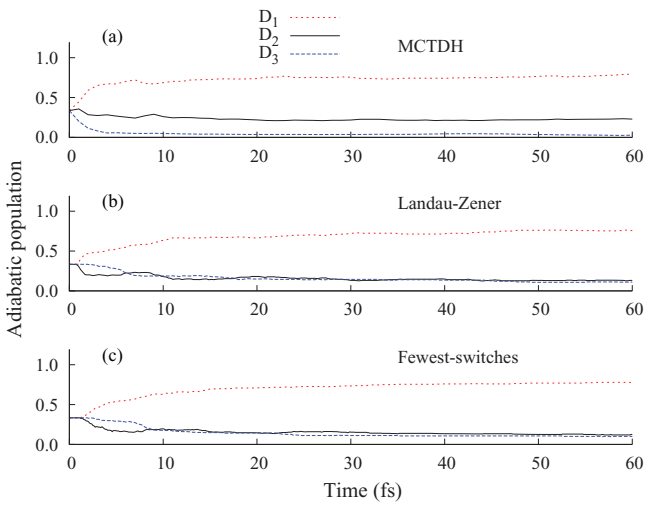

FIG. 4. (a)–(c) Temporal evolution of the electronic population of the three lowest-energy electronic states in adiabatic representation, calculated with MCTDH, Landau-Zener surface hopping, and fewest-switches surface hopping.

is worth mentioning that the PES topology described above will be general to ionized clusters of M···H$^+$···M type featuring strong and symmetrical hydrogen bonds, where M stands for molecules that are able to support hydrogen bonds.

B. Ultrafast Coulomb explosion and correlated proton-hole dynamics

Figure 4 shows the electronic adiabatic states population during the first 60 fs after photoionization. We assume that the ionization cross-section is constant over the range of energies of the three considered electronic states and therefore the results are averaged over propagations starting from each of the three electronic states. In Fig. 4(a) the populations obtained from MCTDH wavepacket propagation are shown. One sees how after 10 to 20 fs the system has mostly decayed to the ground electronic state of the dication.

The agreement between the wavepacket and both types of surface-hopping calculations shown in Figs. 4(b) and 4(c) is rather good. The non-vanishing populations of states D_1 and D_2 reflect the fact that the outgoing H_2O^+ fragment can be in its ground electronic state in which the electron hole corresponds to a π-type orbital, but also to some extent in the first and second excited electronic states, in which the hole is found on the plane of the water cation. It can be noticed that there is some discrepancy in the populations of states B_2 and A_1 in the surface-hopping calculations as compared to the 7D quantum-dynamical calculations. Based on the consistency of the two different switching schemes, we believe that this is an effect of the dimensionality reduction in the quantum dynamics calculations.

Figure 5 depicts the reduced densities in the z and R coordinates obtained from the MCTDH calculation after tracing over the rest of vibrational modes and electronic states. Figures 5(a)–5(c) correspond to calculations with the full diabatic Hamiltonian. In this case the central proton needs about 5 fs to reach the proximity of the oxygen atoms and bounces back to the central position in about 10 fs. Within this timespan the water molecules have not yet started separating due to their larger inertia but there has already been substantial electronic relaxation in which the electron hole localized in one of the water monomers coupled with the motion of the central proton, cf. Fig. 4. In about 30 fs the doubly charged system is found well into the fragmentation channel. Figures 5(d)–5(f) show the evolution of the system under the adiabatic PES without non-adiabatic couplings. In this case an important part of the wavepacket stays trapped close to the Franck-Condon region. The proton and electron hole cannot separate and the system stays bound. This comparison sheds light on the central role of non-adiabatic effects in the fragmentation dynamics of the cluster and its connection with

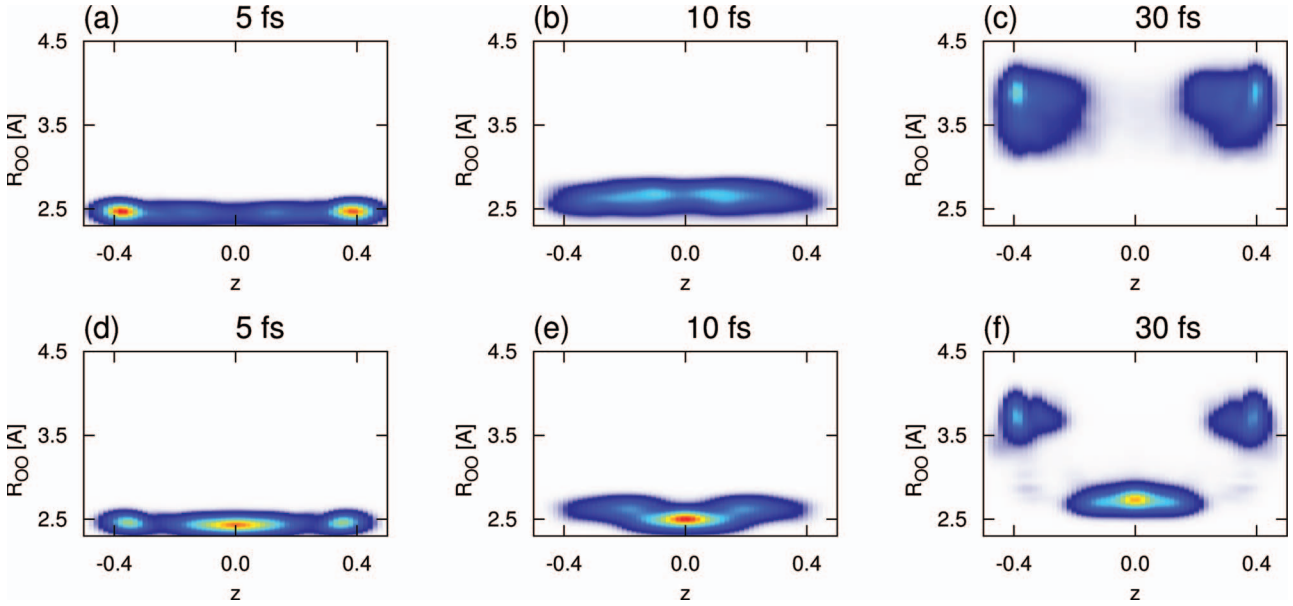

FIG. 5. (a)–(f) Reduced densities in the z (central proton position projected onto the oxygen-oxygen axis) and R (oxygen-oxygen distance) coordinates obtained from the MCTDH calculation after tracing over the rest vibrational modes and all electronic states. The lower panel corresponds to the case in which non-adiabatic coupling is switched off in the Hamiltonian, while the upper panel corresponds to the fully coupled case.

electron hole relaxation coupled to the motion of the central proton.

In order to quantify the correlated proton–hole dynamics we calculate the correlation function between the position of both particles. For the quantum mechanical case, the correlation function is defined as $C_{\rm ph} = S_{\rm ph}/\sqrt{S_{\rm pp}S_{\rm hh}}$, with $S_{xy} = \langle \hat{x}\hat{y}\rangle - \langle \hat{x}\rangle\langle \hat{y}\rangle$. The proton-hole correlation function is calculated in the surface-hopping case analogously by substituting operators by variables and wavefunction averages by ensemble averages over propagated trajectories. $C_{\rm ph}$ is bound to take values between -1, complete anti-correlation, and $+1$, complete correlation. For the excess proton position we take the projection of the central proton position onto the oxygen-oxygen axis. The electron hole position operator is defined as

$$\hat{h} = \frac{1}{2}\hat{R} \otimes (|r\rangle\langle r| - |l\rangle\langle l|) \tag{29}$$

for the wavepacket calculations, where $|l\rangle$ and $|r\rangle$ refer to the two diabatic electronic states with the hole localized on the left- and on the right-hand side water monomers, respectively, and $\hat{R}$ is the position operator corresponding to the oxygen-oxygen distance. In the quantum-classical surface-hopping scenario, we represent the hole straightforwardly as the center of the singly occupied molecular orbital associated with the electronic state on which a particular trajectory is being propagated.

In the Coulomb explosion, as the two like-charged particles, namely, the proton and the electron hole, should be forced to separate due to Coulomb repulsion, a general anti-correlation should be expected that $C_{\rm ph} \leq 0$. In Fig. 6, however, the emergence of a correlation revival at ∼10 fs appears clearly in both quantum-classical and quantum mechanical scenario, with striking quantitative match of the two approaches. The revival is due to the bounce-back dynamics of both proton and hole in the first 10 fs before the water molecules had time to separate.

Thereafter the dication breaks apart with proton and hole localized on either of the separating fragments. This process is made explicit by direct visualization of the proton-hole motion of one of the surface-hopping trajectories in Fig. 7.

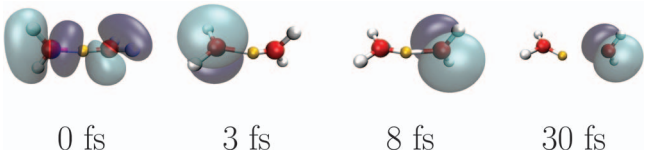

FIG. 7. Direct visualization of motion for the proton (orange) and the electron hole (blue and purple for positive and negative wavefunction values, respectively), when initialized from S_{A_1} state. The geometries were taken at 0, 3, 8, and 30 fs (from left).

C. Photoionization spectrum

The photoionization spectrum was computed by Fourier transform of the autocorrelation function of the propagated wavepacket

$$I(E) \sim E \int_{-\infty}^{\infty} dt\, \langle \Psi(0) \mid \Psi(t)\rangle\, e^{iEt}, \tag{30}$$

where E is the ionization energy. Since we are considering an irreversible process, the spectral features will have an intrinsic width that directly depends on the time-scale of the Coulomb explosion. Figure 8(a) shows the PI spectrum obtained by propagation with the adiabatic Hamiltonian and neglecting the non-adiabatic coupling between the different electronic states. The individual spectra were obtained by populating each of the electronic states at $t = 0$ and incoherently summing to provide the total spectrum. The dotted line relates to the two lowest electronic states of the dication. As discussed above, ionization and further evolution in the lowest electronic state leads to an ultrafast fragmentation. This corresponds to the broad feature between 20 and 21 eV, which fully develops in the first 10 fs. In particular, the FWHM of the peak (∼0.6 eV) corresponds to a process with time scale of ∼12 fs, implying rapid fragmentation after the photoionization. Above 21 eV the spectrum abruptly transitions into a region with bound vibrational states supported above the lower energy conical intersection. The separation between the peaks is about 650 $\rm cm^{-1}$, corresponding to bound water-water vibration. The shoulder above 22 eV corresponds to a small fraction of the wavepacket that finds its way into the

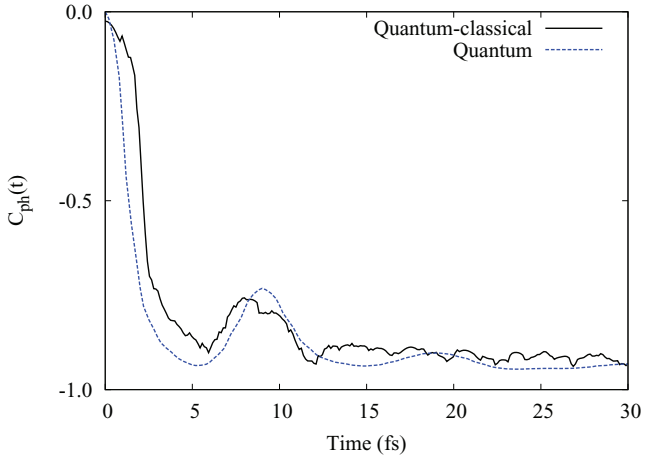

FIG. 6. Correlation function between proton and electron hole positions obtained from MCTDH and surface-hopping calculations.

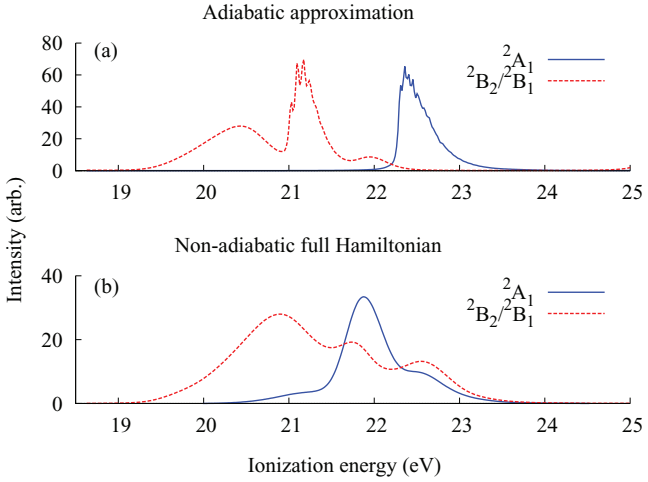

FIG. 8. Photoionization spectra calculated from adiabatic dynamics (a) and from non-adiabatic dynamics (b).

fragmentation channel from the first excited state of the dication. The solid line in Fig. 8(a) corresponds to ionization into the second excited electronic state of the dication. Bound vibrational states exist on its PES, as seen by the peaks in the spectrum at about 23 eV. Hence, even though $H_5O_2^{2+}$ is doubly charged, the missing non-adiabatic coupling between nuclei and electrons can significantly prevent the Zundel dication from fragmenting and relaxing via Coulomb repulsion. The calculation of the PI spectrum with the full vibronic Hamiltonian results in a broad, continuous band with three differentiated peaks in the range 20–24 eV as shown in Fig. 8(b). This feature arises from the strong mixing of the three lowest electronic states of the dication and the fact that in the coupled case the dication has no bound vibrational states. To finalize this discussion we note that we calculated the PI spectrum based on PES at the Hartree-Fock-Koopmans level of theory and compared it to the CASSCF based spectrum. The two spectra were found to be very similar in their features and intensities indicating that Hartree-Fock-Koopmans potentials reproduce the conical intersections and overall shape of the PES remarkably well, at least in the vicinity of the Franck-Condon region for the set of outer-valence electronic states considered here.

D. Kinetic energy release of the fragments

The KER spectrum reflects the asymptotic energy redistribution between the fragmentation mode, in this case the water-water distance coordinate and the internal coordinates of the fragments. In Fig. 9 we present the KER of the H_3^+O and H_2O^+ fragments obtained from the 7D quantum dynamical calculation, as well as from reduced 7D and full dimensional models using the surface-hopping method. In the wavepacket calculation, the KER spectrum is obtained from the quantum flux analysis of the outgoing wavepacket through a complex absorbing potential placed in the outgoing channel.[11] For the surface hopping calculations we find a shift of about 2 eV of the KER spectrum to higher energies in the 15D case in comparison to the 7D case, which indicates energy redistribution from internal modes of the monomers to the dissociation coordinate. A reasonable agreement is found between the full quantum and surface-hopping KER for the 7D case. A similar shift would then be expected for full quantum-dynamical calculations and indicates that the modes neglected in the 7D model may become active shortly after the photoionization process. The fact that other observables as the electronic state populations and the correlation function nicely agree between the quantum 7D and the surface-hopping calculations suggest that both types to calculations provide the same overall physical picture. The broader envelope of the quantum KER spectrum is probably a consequence of the initial conditions sampling in the surface-hopping calculations, which are not able to capture zero point energy effects.

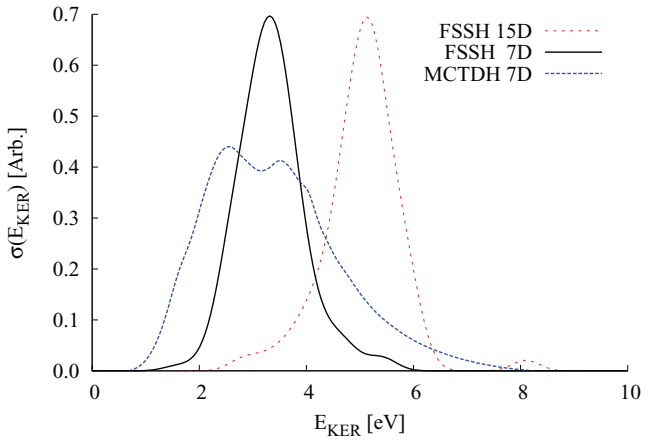

FIG. 9. Kinetic energy release (KER) spectra of the outgoing fragments H_3^+O and H_2O^+ after tracing over the three lowest energy states, obtained from full dimensional quantum-classical treatment, and reduced dimensional quantum-classical/quantum-mechanical treatment, respectively.

E. Ionization into the higher outer-valence ionic states

To a good approximation, each water molecule in the Zundel cation contributes three outer-valence orbitals with six electrons to the cluster. Therefore, there exist three further excited electronic states of $H_5O_2^{2+}$ of outer-valence character above the three lowest states considered up to now. However, it becomes increasingly cumbersome to obtain a diabatic representation of the Hamiltonian with even more coupled states for a quantum-dynamical treatment and, moreover, the upper states lead to further fragmentation channels beyond the two body fragmentation discussed above, which would require a full dimensional treatment and very extended grids. Such type of calculations are not within reach at the moment. Therefore, we study the dynamics in the complete outer-valence set of lowest energy electronic states of $H_5O_2^{2+}$ using surface-hopping and propagate 100 trajectories starting from every electronic state. The six lowest energy electronic states of $H_5O_2^{2+}$ span the range of ionization potential at the Franck-Condon point from 20.6 eV to 27.4 eV calculated at the CASSCF level. The six states are predominantly one-hole states, and only states above the set of outer-valence states involve one-particle-two-hole configurations in which one electron is further excited to an unoccupied orbital. For such higher-energy inner-valence states the Koopmans' theorem no longer applies.

Figure 10 presents the branching ratios of several two- and three-body channels calculated by surface hopping. In order to calculate the branching rations we analyze the positions of the hydrogen atoms with respect to the oxygen atoms at the end of each trajectory and consider that they are bound if they are found within an acceptance ratio slightly larger than a typical O–H bond. For a higher initial electronic excitation more channels become energetically accessible. In contrast to the dynamics initialized from the three low-energy ionic states, which merely gives two-body fragmentation

$$H^+(H_2O)_2 + \gamma \rightarrow H_2O^+ + H_3O^+ + e^-,$$

the branching ratio of three-body fragmentation channels

$$H^+(H_2O)_2 + \gamma \rightarrow H^+ + H_2O + H_2O^+ + e^-,$$

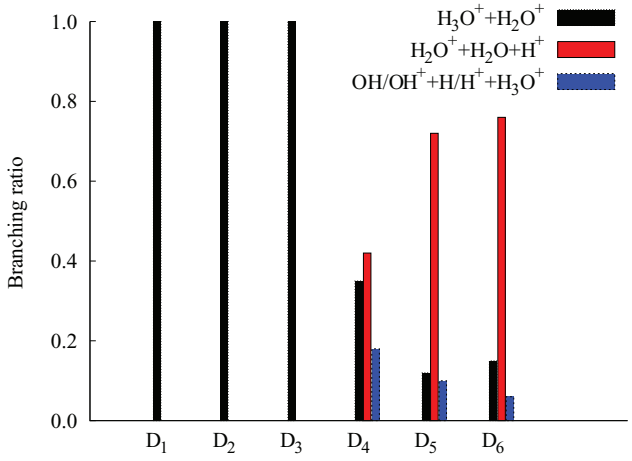

FIG. 10. Branching ratio of two- and three-fragment channels, initialized from outer-valence ionic states.

$$H^+(H_2O)_2 + \gamma \rightarrow H^+ + OH + H_3O^+ + e^-,$$

$$H^+(H_2O)_2 + \gamma \rightarrow H + OH^+ + H_3O^+ + e^-$$

becomes important and can even exceed that of the two-body channel. We conclude that photon energies under about 24 eV will lead in all cases to a fast two-body fragmentation of the cluster. An increase in energy to about 27 eV, in which still the outer-valence is being ionized, will lead to further fragmentation channels in which the external hydrogen atoms of the cluster can be ejected during the Coulomb explosion.

IV. CONCLUSION

In the present work, we thoroughly investigated the strongly non-adiabatic Coulomb explosion of the Zundel cation after outer-valence ionization by XUV light. We analyzed in detail the mechanism of fragmentation in the three lowest energy electronic states of $H_5O_2{}^{2+}$. For this set of electronic states, we constructed a diabatic Hamiltonian in 7D from CASSCF quality PESs, which was used in quantum-dynamical calculations of the fragmentation process with the MCTDH method. We found that the three lowest electronic states are coupled by strong non-adiabatic effects in which the motion of the central proton along the hydrogen bond between the two water molecules plays a fundamental role. When the dynamics after ionization were analyzed, we found a fast and anti-correlated motion of the central proton and the electron hole that localizes them at opposite sides of the cluster and leads to a Coulomb explosion within femtoseconds. Exactly the same mechanism and time-scales were reproduced by surface-hopping calculations on PESs of the same quality. The vibrationally resolved photoionization spectrum of the cluster was also provided for the first time in the range between 19 to 24 eV by quantum-dynamical calculations. This energy range covers the lowest energy part of the outer-valence spectrum, which extends up to about 27 eV. The complete outer-valence ionized states of $H_5O_2{}^{2+}$ comprises six electronic states. The dynamics in this set of coupled electronic states was calculated by surface-hopping. We found that above the lowest three electronic states, fragmentation into other than the two-body channel is possible and even dominant. The dynamics starting from the upper states are also strongly non-adiabatic and a large fraction of the initially available electronic energy is redistributed into vibrational modes, which explains the possibility of further fragmentation.

Our calculations provide an in-depth analysis of the coupled electronic and nuclear non-Born-Oppenheimer dynamics in a small ionized water cluster, in which the high mobility of proton and electron hole play a fundamental role. The good agreement between quantum and surface-hopping treatments paves the way for future explorations of larger clusters and the liquid phase.

ACKNOWLEDGMENTS

We are grateful to the Helmholtz Gemeinschaft for financial support through the virtual institute "Dynamic Pathways in Multidimensional Landscapes" and to Professor Robin Santra for inspiring discussions.

[1]G. A. Worth and L. S. Cederbaum, Annu. Rev. Phys. Chem. **55**, 127 (2004).
[2]G. A. Worth, P. Hunt, and M. A. Robb, J. Phys. Chem. A **107**, 621 (2003).
[3]G. Worth and M. A. Robb, Adv. Chem. Phys. **124**, 355 (2002).
[4]H. C. Longuet-Higgins, U. Opik, M. H. L. Pryce, and R. A. Sack, Proc. R. Soc. London, Ser. A **244**, 1 (1958).
[5]H. Köppel, W. Domcke, and L. S. Cederbaum, Adv. Chem. Phys. **57**, 59 (1984).
[6]U. Manthe, H.-D. Meyer, and L. S. Cederbaum, J. Chem. Phys. **97**, 3199 (1992).
[7]Z. Vager, R. Naaman, and E. P. Kanter, Science **244**, 426 (1989).
[8]H. Shinohara, N. Nishi, and N. Washida, J. Chem. Phys. **84**, 5561 (1986).
[9]Y. V. Novakovskaya, Int. J. Quantum Chem. **107**, 2763 (2007).
[10]F. Dong, S. Heinbuch, J. J. Rocca, and E. R. Bernstein, J. Chem. Phys. **124**, 224319 (2006).
[11]M. H. Beck, A. Jäckle, G. A. Worth, and H.-D. Meyer, Phys. Rep. **324**, 1 (2000).
[12]W. H. Miller, J. Phys. Chem. A **105**, 2942 (2001).
[13]J. Jornet-Somoza, B. Lasorne, M. Robb, H. Meyer, D. Lauvergnat, and F. Gatti, J. Chem. Phys. **137**, 084304 (2012).
[14]I. Burghardt, K. Giri, and G. A. Worth, J. Chem. Phys. **129**, 174104 (2008).
[15]J. C. Tully, J. Chem. Phys. **93**, 1061 (1990).
[16]B. R. Landry and J. E. Subotnik, J. Chem. Phys. **135**, 191101 (2011).
[17]L. Lammich, C. Domesle, B. Jordon-Thaden, M. Förstel, T. Arion, T. Lischke, O. Heber, S. Klumpp, M. Martins, N. Guerassimova, R. Treusch, J. Ullrich, U. Hergenhahn, H. B. Pedersen, and A. Wolf, Phys. Rev. Lett. **105**, 253003 (2010).
[18]Z. Li, M. E. Madjet, O. Vendrell, and R. Santra, Phys. Rev. Lett. **110**, 038302 (2013).
[19]O. Vendrell, F. Gatti, D. Lauvergnat, and H.-D. Meyer, J. Chem. Phys. **127**, 184302 (2007).
[20]L. Doriol, B. Lasorne, F. Gatti, M. Schröder, O. Vendrell, and H. Meyer, Comput. Theor. Chem. **990**, 75 (2012).
[21]O. Vendrell, M. Brill, F. Gatti, D. Lauvergnat, and H.-D. Meyer, J. Chem. Phys. **130**, 234305 (2009).
[22]B. O. Roos, P. R. Taylor, and P. E. M. Siegbahn, Chem. Phys. **48**, 157 (1980).
[23]P. E. M. Siegbahn, J. Almlöf, A. Heiberg, and B. O. Roos, J. Chem. Phys. **74**, 2384 (1981).
[24]T. H. Dunning, J. Chem. Phys. **90**, 1007 (1989).
[25]S. Carter, S. J. Culik, and J. M. Bowman, J. Chem. Phys. **107**, 10458 (1997).
[26]J. M. Bowman, S. Carter, and X. Huang, Int. Rev. Phys. Chem. **22**, 533 (2003).

[27]V. Veryazov, P.-O. Widmark, L. Serrano-Andres, R. Lindh, and B. Roos, Int. J. Quantum Chem. **100**, 626 (2004).
[28]H. Köppel, J. Gronki, and S. Mahapatra, J. Chem. Phys. **115**, 2377 (2001).
[29]H. Köppel and B. Schubert, Mol. Phys. **104**, 1069 (2006).
[30]H. Köppel, Faraday Discuss. **127**, 35 (2004).
[31]E. V. Gromov, C. Lévêque, F. Gatti, I. Burghardt, and H. Köppel, J. Chem. Phys. **135**, 164305 (2011).
[32]*Multidimensional Quantum Dynamics: MCTDH Theory and Its Applications*, edited by H.-D. Meyer, F. Gatti, and G. Worth (Wiley-VCH, 2009).
[33]G. A. Worth, M. H. Beck, A. Jäckle, and H.-D. Meyer, The MCTDH package, version 8.2, 2000; H.-D. Meyer, version 8.3, 2002; version 8.4, 2007; see http://mctdh.uni-hd.de.
[34]A. Jäckle and H.-D. Meyer, J. Chem. Phys. **104**, 7974 (1996).
[35]A. Jäckle and H.-D. Meyer, J. Chem. Phys. **109**, 3772 (1998).
[36]H.-D. Meyer and G. A. Worth, Theor. Chem. Acc. **109**, 251 (2003).
[37]H.-D. Meyer, F. Le Quéré, C. Léonard, and F. Gatti, Chem. Phys. **329**, 179 (2006).
[38]R. Kosloff and H. Tal-Ezer, Chem. Phys. Lett. **127**, 223 (1986).
[39]M. G. H. Boogaarts, P. C. Hinnen, and G. Meijer, Chem. Phys. Lett. **223**, 537 (1994).
[40]U. V. Riss and H.-D. Meyer, J. Chem. Phys. **105**, 1409 (1996).
[41]U. Manthe and H. Köppel, J. Chem. Phys. **93**, 345 (1990).
[42]I. Tavernelli, B. F. E. Curchod, and U. Rothlisberger, Phys. Rev. A **81**, 052508 (2010).
[43]G. A. Jones, B. K. Carpenter, and M. N. Paddon-Row, J. Am. Chem. Soc. **120**, 5499 (1998).
[44]A. I. Voronin, J. M. C. Marques, and A. J. C. Varandas, J. Phys. Chem. A **102**, 6057 (1998).
[45]E. Tapavicza, U. Tavernelli, C. Rothlisberger, C. Fillipi, and M. E. Casida, J. Chem. Phys. **129**, 124108 (2008).
[46]A. D. Hammerich, U. Manthe, R. Kosloff, H.-D. Meyer, and L. S. Cederbaum, J. Chem. Phys. **101**, 5623 (1994).
[47]S. Hammes-Schiffer and J. C. Tully, J. Chem. Phys. **101**, 4657 (1994).
[48]E. Fabiano, T. W. Keal, and W. Thiel, Chem. Phys. **349**, 334 (2008).
[49]J. Pittner, H. Lischka, and M. Barbatti, Chem. Phys. **356**, 147 (2009).
[50]M. S. Topaler, T. C. Allison, D. W. Schwenke, and D. G. Truhlar, J. Phys. Chem. A **102**, 1666 (1998).
[51]H. C. Andersen, J. Comput. Phys. **52**, 24 (1983).
[52]T. Koopmans, Physica **1**, 104 (1934).